ATLAS NOTE

ATL-PHYS-PUB-2016-006

29th January 2016

Study of higher-order QCD corrections in the gg→H→VV process

The ATLAS Collaboration

Abstract

Several studies have shown that the high-mass off-peak regions in the $H \to ZZ$ and $H \to WW$ channels above the VV mass threshold ($V = W, Z$) have sensitivity to off-shell Higgs production and interference effects. This feature can be exploited to characterize the Higgs boson off-shell signal strength and its associated couplings. This note reports on the treatment of the QCD-related systematic uncertainties for the extraction of the off-shell Higgs boson signal strength related to the comparison of different Monte Carlo modeling for the gg-initiated processes, gg→ (H^*) →VV. Higher-order QCD corrections to the transverse momentum p_{T} and the rapidity y of the VV system are studied using Sherpa+OpenLoops, which includes matrix-element calculations for the first hard jet emission. A difference of the order of 20% in the ratio of the p_{T} of the VV system in the relevant kinematic region is observed when comparing the LO generators with parton shower to Sherpa+OpenLoops, while the difference in the rapidity of the VV system is found to be small.

ATL-PHYS-PUB-2016-006
29 January 2016

1 Introduction

Measurements of the ZZ and WW final states in the high mass can be used to extract the off-shell coupling strength of the Higgs boson [1–3]. The analyses [4, 5] present constraints on the off-shell Higgs boson event yields normalized to the Standard Model prediction (signal strength) in the ZZ→4ℓ, ZZ→2ℓ2ν and WW→ $\ell\nu\ell\nu$ channels. In the ATLAS analysis [5], using the CLs method, the observed 95% confidence level (CL) upper limit on the off-shell signal strength is in the range 5.1–8.6, with an expected range of 6.7–11.0. This range is determined by varying the unknown gg→ZZ and gg→ WW background K-factor from higher-order QCD corrections between half and twice the value of the evaluated signal K-factor. Under the assumption that the Higgs boson couplings are independent of the energy scale of the Higgs production, a combination of the off-shell constraint with the on-shell Higgs peak measurement yields an observed (expected) 95% CL upper limit the Higgs total width normalized to the one of the Standard Model, i.e. $\Gamma_{\rm H}/\Gamma_{\rm SM}$, in the range 4.5–7.5 (6.5–11.2) employing the same variations of the background K-factor. Assuming that the unknown gg→VV background K-factor is equal to the signal K-factor, this translates into an observed (expected) 95% CL upper limit on the Higgs boson total width of 22.7 (33.0) MeV.

The analysis [5] employed to extract the off-shell signal strength in the high mass ($m_{4\ell}$ >220 GeV) ZZ→4ℓ, ZZ→2ℓ2ν and WW→ $\ell\nu\ell\nu$ final states, is based on two Monte Carlo simulations for gg-initiated processes, namely gg2VV [6] and MCFM [3]. The dominant gg-initiated processes used in the analysis [5] are listed below:

1. gg→ H → ZZ, the signal (S) comprising both the on-shell peak at $m_{\rm H}$ =125.5 GeV and the off-shell region where the Higgs boson acts as a propagator;
2. gg→ ZZ, the continuum background (B);
3. gg→ (H^*) → ZZ, the signal, continuum background and interference contribution, labelled as SBI in what follows.

However, only Lowest-Order (LO) in QCD Monte Carlo simulations are available, namely gg2VV and MCFM with Pythia8 [7] showering. For this reason, mass-dependent K-factors to higher order accuracy are needed to achieve a better precision.

- For the signal process, higher order QCD corrections are computed: LO to Next-to-Next-to-Leading-Order (NNLO) K-factors are calculated as a function of the diboson invariant mass $m_{\rm ZZ}$.
- For the background process, the full K-factor from LO to NNLO accuracy is currently not available.

Different approaches exploited in order to take into account the absence of higher order QCD corrections in gg→ (H^*) →VV final states (it is to note that Next-to-Leading Order, NLO, gg→ZZ QCD calculation has been recently performed [8]) and the systematic uncertainties associated to these processes will be detailed in the following Sections.

2 Parton Shower Scheme Dependence

Given that no higher order matrix element calculations are available for the gg-initiated processes, the only way to simulate QCD radiation is through the parton shower. However, as the generation is done at LO in

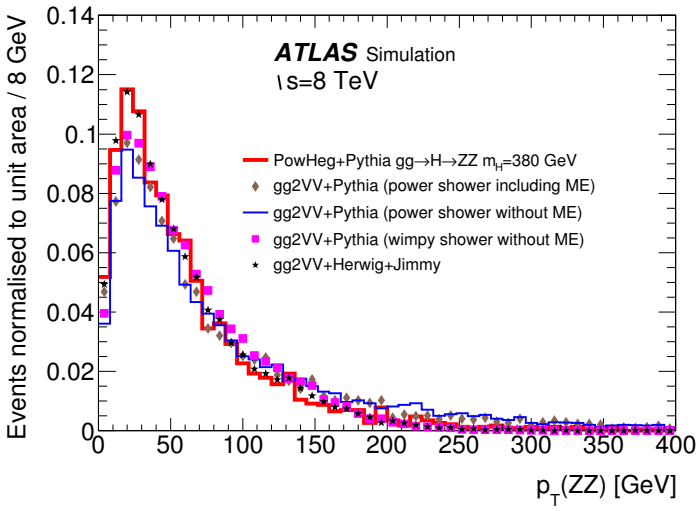

Figure 1: Distribution of p_{T}(ZZ) comparing the NLO generator Powheg showered with Pythia8, the LO generator gg2VV + Pythia (power or wimpy shower), the LO generator gg2VV showered with Jimmy+Herwig. All samples are restricted to the range (345< $m_{4\ell}$ <415) GeV.

QCD, there is no clear prescription to evaluate the systematic uncertainties on the QCD scale. According to the maximum jet p_{T} scale emission characterizing the parton showers, two different configurations [9] are exploited, the *power shower* (the emission is allowed up to the kinematical limit) and the *wimpy shower* (the shower is started at the value of the factorization or the renormalization scale). Pythia8 is tuned as default with the power shower option. The comparison is carried out involving the following parton shower schemes at generator level:

- Pythia8 power shower including a matrix element correction on the first jet emission such that information coming from the exact matrix element calculation is exploited for the hardest jet in the shower [7];
- Pythia8 power shower without a matrix element correction;
- Pythia8 wimpy shower without a matrix element correction;
- Herwig6.5 [10] in combination with Jimmy.

The items above are finally compared to high-mass Powheg-Box [11] NLO gg→ H → ZZ event sample with a Higgs boson mass generated with m_{H}=380 GeV, chosen around the most sensitive off-shell invariant mass region for the analysis. The normalized p_{T}(ZZ) distributions, detailed in Figure 1 as reported in Ref. [9] for the sample above in the text are plotted in the same high ZZ mass range (345< $m_{4\ell}$ <415) GeV in order to ensure a compatible mass of the hard interaction system. As the default samples are generated with the LO gg→ (H^*) →ZZ matrix element with Pythia8 using the power shower parton shower option and this sample shows the largest deviation from Powheg, the full difference of the order of 10% is taken as a systematic uncertainty in the ATLAS analysis as in [5].

3 Higher order QCD corrections to the transverse momentum and the rapidity of the ZZ system

Higher order QCD corrections for the gg→ ZZ processes are studied using the Sherpa+OpenLoops [12, 13] generator that contains the LO gg→ZZ+1-jet matrix element and merges this with the LO gg→ZZ+ 0-jet matrix element. For the gg→ H → ZZ signal contribution with m_{H}=380 GeV (on-shell signal), the Powheg generator reweighted (as a function of p_{T}) to the HRes2.1 prediction [14] to reach NNLO+NNLL accuracy is also used. Figures 2, 3 and 4 include validation distributions of various comparisons of the variables of interest, namely the transverse momentum, p_{T}(ZZ), and the rapidity, Y(ZZ), of the ZZ system in both on-shell and off-shell mass regions using Powheg+Pythia8, Sherpa+OpenLoops and gg2VV+Pythia8 generators using kinematic variables computed at truth level. The list of cuts applied in the generation level can be found below (p_{T}^{ℓ} is the transverse momentum of each lepton in the final state, $|\eta^{\ell}|$ represents its rapidity [1] while m_{Z1} is the Z boson mass closest to the Z peak, being m_{Z2} the mass of the second lepton pair):

- $m_{4\ell}$ >100 GeV;
- p_{T}^{ℓ} >3 GeV;
- $|\eta^{\ell}|$ <2.8;
- $m_{\mathrm{Z1,Z2}}$ > 4 GeV.

Additional selection criteria are applied on the final state quadruplet (the leptons in the quadruplet are ordered in transverse momentum and denoted with the superscript ℓ in what follows) in the Monte Carlo samples in such a way to mimic the standard selection reported in Ref. [5], namely:

- $p_{\mathrm{T}}^{\ell 1}$ >20 GeV, $p_{\mathrm{T}}^{\ell 2}$ >15 GeV, $p_{\mathrm{T}}^{\ell 3}$ >10 GeV, $p_{\mathrm{T}}^{\ell 4}$ >5 (6) GeV for muons (electrons);
- $|\eta^{\ell}|$ <2.5;
- (50< m_{Z1} <106) GeV;
- if $m_{4\ell}$ <140 GeV → m_{Z2} >12 GeV, if 140< $m_{4\ell}$ <190 GeV → m_{Z2} >0.76·($m_{4\ell}$-140)+12 GeV, if $m_{4\ell}$ >190 GeV → m_{Z2} >50 GeV.

The errors bars in Figures 2, 3 and 4 indicate the statistical uncertainty related to the finite Monte Carlo statistics only. The systematic uncertainties, when applicable, are drawn as shaded boxes, extracted from scale variations on Sherpa+OpenLoops and HRes2.1 as described in the following Section 3.1. The systematic uncertainties from the HRes2.1 are applicable here as the Powheg generator is directly reweighted to the HRes2.1 prediction. The results and the distributions reported in the following Figures refer to Monte Carlo samples generated at a collision energy $\sqrt{s}$=8 TeV.

As highlighted in Figure 2 (a) for what concerns the on-shell and Figure 2 (b) for the off-shell, the lack of higher QCD calculations in gg2VV results in different p_{T} spectra (order of 20% in the relevant kinematic region) compared to the higher order Powheg and Sherpa+OpenLoops Monte Carlo. In the

[1] ATLAS uses a right-handed coordinate system with its origin at the nominal interaction point (IP) in the centre of the detector, and the z-axis along the beam line. The x-axis points from the IP to the centre of the LHC ring, and the y-axis points upwards. Cylindrical coordinates (r, ϕ) are used in the transverse plane, ϕ being the azimuthal angle around the beam line. Observables labelled *transverse* are projected into the x–y plane. The pseudorapidity is defined in terms of the polar angle θ as η=-ln tan($\frac{\theta}{2}$).

high mass region, the off-shell (generated with m_{H}=125.5 GeV) and on-shell (produced with m_{H}=380 GeV) Higgs productions with gg2VV match fairly well as shown in Figure 2 (b).
Figure 3 (a) shows that the differences in p_{T} between Sherpa and gg2VV in the off-shell high mass region are not fully covered by the uncertainties assigned to Sherpa. Since the Sherpa generator has a better treatment of the first hard jet emission, in the $H \rightarrow ZZ \rightarrow 4\ell$ analysis, gg2VV is reweighted to the Sherpa prediction in the ATLAS analysis [5]. As for the rapidity distribution reported in Figure 3 (b), no significant difference between gg2VV and Sherpa is present in the high mass region; hence, the reweighting procedure on Y is not necessary.
Figures 3 (c) and (d) stress the fact that the ZZ-transverse momentum and the rapidity of the signal process gg$\rightarrow (H^{*}) \rightarrow$ ZZ differ from the gg$\rightarrow$ ZZ background process and the SBI unlike the gg2VV generator as noted in Figures 4 (a) and (b). This is caused by the presence of the additional matrix element correction to the first jet emission included in Sherpa that generates a different treatment of signal and background components. This statement has been explicitly validated by removing the 1-jet matrix element computation in Sherpa: full compatibility is found between signal and background once the 1-jet ME treatment is removed in Sherpa.

In the analysis deployed by ATLAS [5], the LO gg2VV generator, whose p_{T} and y distributions are displayed in Figures 4, is reweighted to Sherpa+OpenLoops in the p_{T} of the VV system to achieve a better description of the p_{T} spectrum: the impact of the reweighting on the acceptance is calculated to be below 1% for the signal and at the level of 4-6% for the background. In the ZZ$\rightarrow 4\ell$ channel, the reweighting procedure is only used to account for the acceptance effects, as the matrix-element discriminant employed to disentangle signal and background components is insensitive to the p_{T} of the ZZ system. For the ZZ$\rightarrow 2\ell 2\nu$ channel, the reweighting is applied in both the transverse mass shape and acceptance as the m_{T} holds dependence on the transverse momentum of the ZZ system.

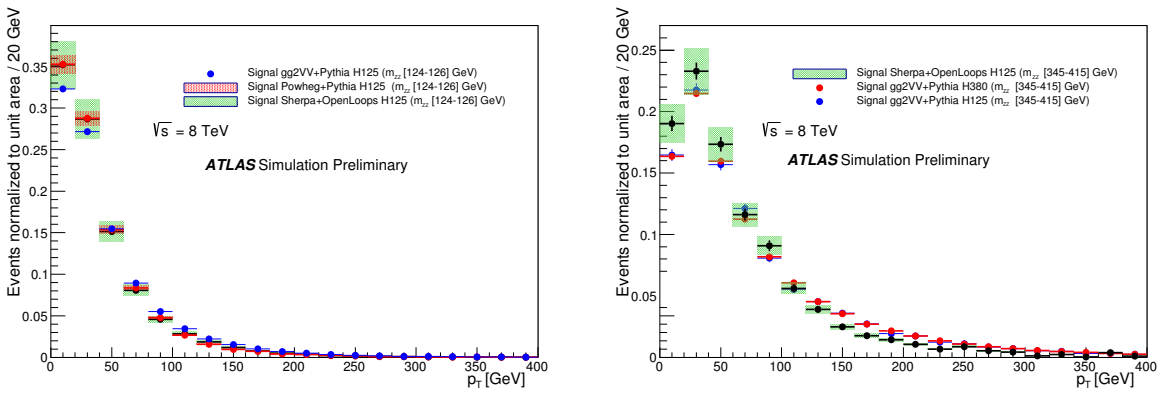

(a) (b)

Figure 2: Comparison of the on-shell gg$\rightarrow (H^{*}) \rightarrow$ ZZ signal process in p_{T} (a) generated with m_{H}=125.5 GeV in the mass range $m_{ZZ} \in$ [124,126] GeV for Powheg, Sherpa and gg2VV. Comparison of the gg$\rightarrow (H^{*}) \rightarrow$ ZZ off-shell signal process in p_{T} (b) with m_{H}=125.5 GeV produced with gg2VV and Sherpa and gg$\rightarrow (H^{*}) \rightarrow$ ZZ signal process with m_{H}=380 GeV using gg2VV (on-shell) in the region $m_{ZZ} \in$ [345,415] GeV.

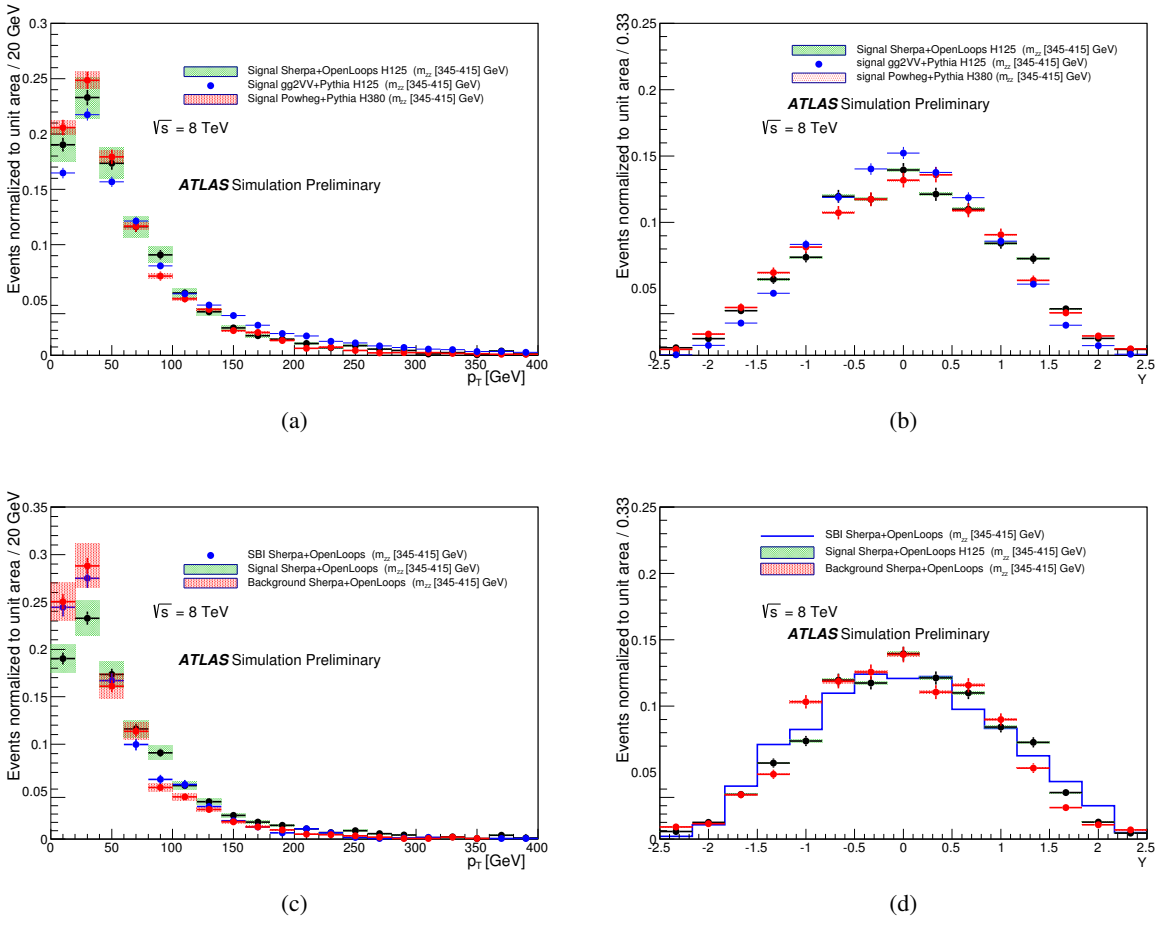

Figure 3: Comparison of the gg→ (H^*) → ZZ off-shell signal process in p_{T} (a) and rapidity (b) generated with m_{H}=125.5 GeV produced with gg2VV and Sherpa and gg→ (H^*) → ZZ signal process with m_{H}=380 GeV using Powheg (on-shell) in the region $m_{ZZ} \in$ [345,415] GeV. Off-shell comparison in p_{T} (c) and rapidity (d) of the gg→ (H^*) → ZZ signal sample generated with m_{H}=125.5 GeV, the gg→ ZZ background and the SBI contribution using Sherpa in the mass range $m_{ZZ} \in$ [345,415] GeV.

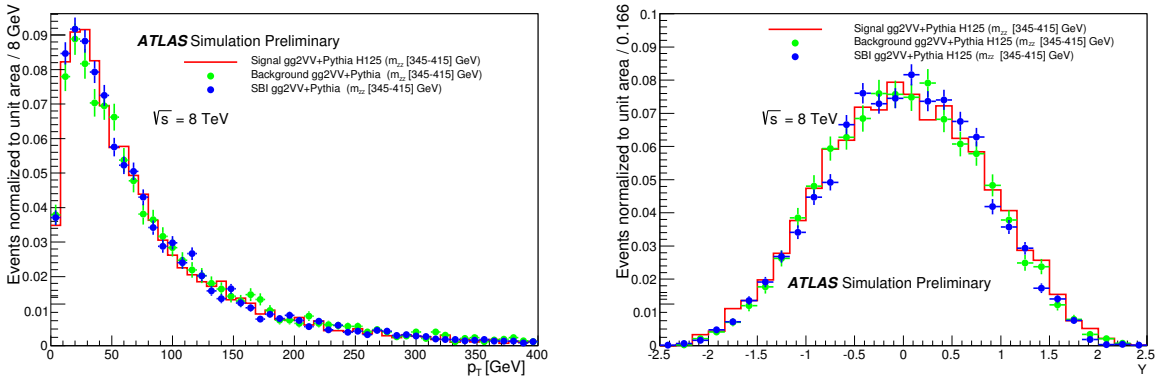

(a) (b)

Figure 4: Comparison in p_{T} (a) and rapidity (b) of the three gg2VV contributions (signal generated with m_{H}=125.5 GeV, background and SBI) in the mass region $m_{\mathrm{ZZ}} \in$ [345,415] GeV.

3.1 Scale variations on the gg-initiated samples

In order to evaluate the systematic effects on the uncertainties on p_{T} and η in the ZZ frame, the procedure is applied by varying the renormalisation scale (μ_{R}), the factorization scale (μ_{F}), the resummation scale (μ_{Q}) and the resummation scale related to the bottom quark mass (μ_{B}).

The impact of the PDF uncertainties is also evaluated: the nominal PDF set, CT10 [15], applied on the Powheg signal sample at m_{H}=125.5 GeV are compared with MSTW2008 [16] and with NNPDF2.3 [17] in bins of ZZ-transverse momentum and rapidity. Its impact is found to be below 3%. The Monte Carlo simulations employed for these studies and the full scheme of scale variations applied to these samples are listed in Table 1. Assuming that the resummation scales (μ_{Q} and μ_{B}) variations are independent of the normalization and factorization scales (μ_{R} and μ_{F}), we fix the vector pair (μ_{R}, μ_{F}) while varying μ_{Q} or μ_{B}. Similarly we fix the resummation scales, μ_{Q} and μ_{B}, while varying μ_{R} and μ_{F}. Following the usual prescriptions, the nominal scale of the process is set to $m_{\mathrm{ZZ}}/2$ while the nominal value for the resummation scale related to the bottom mass is set to m_{b} and the Powheg nominal values for renormalisation and factorization scales are set to m_{ZZ}.

Figure 5 shows the shape-only variations on p_{T}(ZZ) and Y(ZZ) for a high mass m_{H}=380 GeV gg$\rightarrow H \rightarrow$ ZZ signal process, produced by QCD scale variations evaluated with the HRes2.1 Monte Carlo generator. The scale variations on the rapidity in Figure 5 (b) can be neglected since they are much smaller than those of the transverse momentum, Figure 5 (a). Figure 6 shows the variation of the signal process (a) and the background processes on p_{T}(ZZ) created with the Sherpa+OpenLoops Monte Carlo sample. The envelope of these independent variations on p_{T}(ZZ) is calculated as the maximal up and down contribution for each p_{T} bin for the HRes2.1 case as well as for Sherpa signal and background. Since the contribution of the resummation scale is dominant, a first envelope encompassing renormalisation and factorization scales summed it in quadrature with the envelope extracted from the resummation scale provides enough accuracy for this study. Note that the Sherpa variations enclose the variations of HRes2.1 because Sherpa does not contain the full NLO calculations, hence its variations are larger than the typical scales of HRes2.1.The systematic uncertainties reported in Ref. [5] associated with the Sherpa-based reweighting

Process	MC	Nominal Scales	Scale variations	# Variations
$gg \to H \to ZZ$	HRes	$\mu_R = \mu_F = \frac{m_{ZZ}}{2}$	$(\frac{1}{2}\mu_{R/F}, 2\mu_{R/F})$, $\frac{1}{2} \leq \mu_F/\mu_R \geq 2$	6
		$\mu_Q = m_{ZZ}/2$, $\mu_B = m_b$	$(\frac{1}{2}\mu_Q, 2\mu_Q)$, $(\frac{1}{4}\mu_B, 4\mu_B)$	8
$gg \to H \to ZZ$	Sherpa	$\mu_R = \mu_F = \frac{m_{ZZ}}{2}$	$(\frac{1}{2}\mu_{R/F}, 2\mu_{R/F})$, $\frac{1}{2} \leq \mu_F/\mu_R \geq 2$	6
		$\mu_Q = m_{ZZ}/2$, $\mu_B = m_b$	$(\frac{1}{\sqrt{2}}\mu_Q, \sqrt{2}\mu_Q)$	2
$q\bar{q} \to ZZ$	Powheg	$\mu_R = \mu_F = m_{ZZ}$	$(\frac{1}{2}\mu_{R/F}, 2\mu_{R/F})$	6

Table 1: Scale variations considered in the evaluation of the theoretical uncertainties related to the p_T(ZZ) and Y(ZZ) for the $gg \to H \to$ZZ and $q\bar{q} \to$ZZ processes. The scale variations on Sherpa signal detailed in the second row are also applied on the Sherpa gg→ZZ continuum background as stated in the text. The merging scale for Sherpa has not been modified for this study.

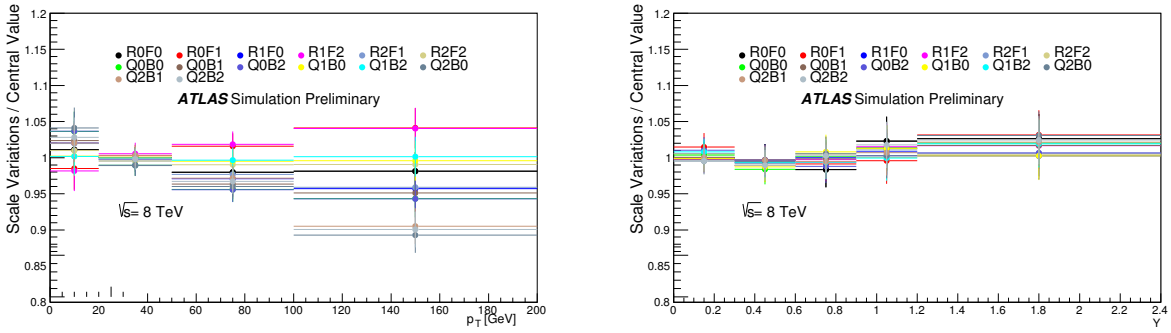

(a) (b)

Figure 5: Relative change of the p_T and Y spectra due to the QCD scale variations produced with HRes2.1 signal generated at m_H=380 GeV: ratio of the up or down variations p_T or rapidity with respect to the nominal distribution. Q labels the resummation scale, B the resummation scale related to the bottom quark mass, R the renormalisation scale, F the factorization scale. The numbers coupled with each variation characterize the nominal value (1), the down variation (0) and the up variation (2).

in p_T of the VV system are assessed by varying the relevant scales in Sherpa: the larger in value between the scale variations in Sherpa and 50% of the difference between Sherpa and gg2VV+Pythia is assigned as the systematic uncertainty. This conservative approach is chosen to consider potential uncertainties not accounted for by the scale variations. The impact of the PDF uncertainties is found to be negligible.

4 Summary

Higher-order QCD corrections to the transverse momentum p_T and the rapidity y of the VV system are studied using Sherpa+OpenLoops, which includes matrix-element calculations for the first hard jet emission. A difference of order 20% in the ratio of the p_T of the VV system in the relevant kinematic region is observed when comparing the LO generators with parton shower to Sherpa+OpenLoops, while the difference in the rapidity y of the VV system is small. This difference in the p_T of the VV system can modify the kinematic observables used in the analyses, leading to variations in both the kinematic shapes and acceptance. To account for these effects, the LO generators can be reweighted to Sherpa+OpenLoops

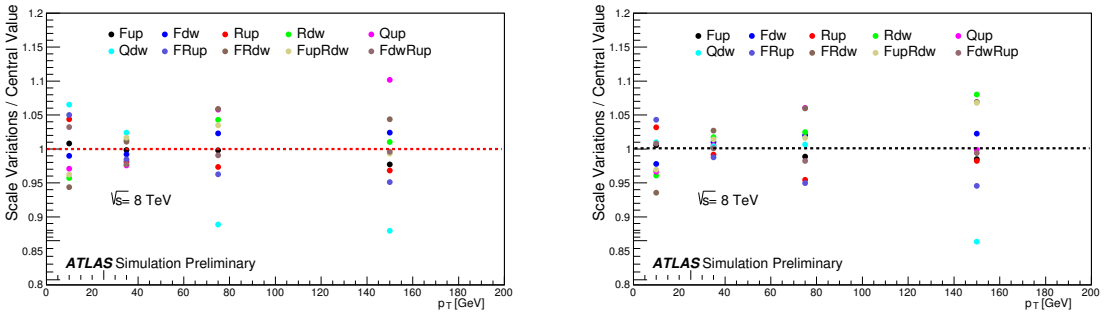

(a) (b)

Figure 6: Relative uncertainties on the p_{T} spectrum for the Sherpa+OpenLoops signal (a) and background (b) samples induced by the QCD scale variations: ratio of the up or down variations with respect to the nominal distribution. Q labels the resummation scale, R the renormalisation scale, F the factorization scale.

in the p_{T} of the VV system. The systematic uncertainties associated with the Sherpa-based reweighting in p_{T} of the VV system are assessed by varying the renormalisation, factorisation and resummation scales in Sherpa, while the PDF uncertainty was found to be small.

References

[1] N. Kauer and G. Passarino,
Inadequacy of zero-width approximation for a light Higgs boson signal, JHEP **08** (2012) 116, arXiv: 1206.4803 [hep-ph].

[2] F. Caola and K. Melnikov, *Constraining the Higgs boson width with ZZ production at the LHC*, Phys. Rev. **D88** (2013) 054024, arXiv: 1307.4935 [hep-ph].

[3] J. M. Campbell, R. K. Ellis and C. Williams,
Bounding the Higgs width at the LHC using full analytic results for $gg \to e^- e^+ \mu^- \mu^+$,
JHEP **04** (2014) 060, arXiv: 1311.3589 [hep-ph].

[4] CMS Collaboration,
Constraints on the Higgs boson width from off-shell production and decay to Z-boson pairs,
Phys. Lett. **B736** (2014) 64, arXiv: 1405.3455 [hep-ex].

[5] ATLAS Collaboration, *Constraints on the off-shell Higgs boson signal strength in the high-mass ZZ and WW final states with the ATLAS detector*, Eur. Phys. J. **C75** (2015) 335,
arXiv: 1503.01060 [hep-ex].

[6] N. Kauer, *Interference effects for $H \to WW/ZZ \to \ell\bar{\nu}_\ell\bar{\ell}\nu_\ell$ searches in gluon fusion at the LHC*,
JHEP **12** (2013) 082, arXiv: 1310.7011 [hep-ph].

[7] T. Sjostrand, S. Mrenna and P. Skands, *A brief introduction to Pythia 8.1*,
Comput.Phys.Commun. **178** (2008) 852, arXiv: 0710.3820 [hep-ph].

[8] F. Caola et al., *QCD corrections to ZZ production in gluon fusion at the LHC*,
Phys. Rev. **D92** (2015) 094028, arXiv: 1509.06734 [hep-ph].

[9] ATLAS Collaboration, *Determination of the off-shell Higgs boson signal strength in the high-mass ZZ final state with the ATLAS detector*, ATLAS-CONF-2014-042 (2014).

[10] G. Corcella et al., *HERWIG 6: An Event generator for hadron emission reactions with interfering gluons (including supersymmetric processes)*, JHEP **010** (2001).

[11] S. Alioli et al., *NLO Higgs boson production via gluon fusion matched with shower in POWHEG*,
JHEP **04** (2009) 002, arXiv: 0812.0578 [hep-ph].

[12] T. Gleisberg et al., *Event generation with SHERPA 1.1*, JHEP **02** (2009) 007,
arXiv: 0811.4622 [hep-ph].

[13] G. Cascioli et al., *Scattering Amplitudes with Open Loops*, Phys. Rev. Lett. **011** (2011),
arXiv: 1111.5206 [hep-px].

[14] D. de Florian et al., *Higgs boson production at the LHC: transverse momentum resummation effects in the $H \to 2\gamma, H \to WW \to l\nu l\nu$ and $H \to ZZ \to 4l$ decay modes*, JHEP **06** (2012) 132,
arXiv: 1203.6321 [hep-ph].

[15] J. Gao et al., *CT10 next-to-next-to-leading order global analysis of QCD*,
Phys. Rev. **D89** (2014) 033009, arXiv: 1302.6246 [hep-ph].

[16] A. Martin et al., *Parton distributions for the LHC*, Eur. Phys. J. **C63** (2009) 189,
arXiv: 0901.0002 [hep-ph].

[17] R. D. Ball et al., *Parton distributions with LHC data*, Nucl. Phys. **B867** (2013) 244,
arXiv: 1207.1303 [hep-ph].